NANO LETTERS

Letter

pubs.acs.org/NanoLett

Mechanical Model of Vertical Nanowire Cell Penetration

Xi Xie,[†] Alexander M. Xu,[†] Matthew R. Angle,[†] Noureddine Tayebi,[‡] Piyush Verma,[†] and Nicholas A. Melosh*,[†]

[†]Department of Materials Science and Engineering, Stanford University, Stanford, California 94305, United States

[‡]Intel Inc., 220 Mission College Boulevard, Santa Clara, California 95054, United States

Supporting Information

ABSTRACT: Direct access into cells' interiors is essential for biomolecular delivery, gene transfection, and electrical recordings yet is challenging due to the cell membrane barrier. Recently, molecular delivery using vertical nanowires (NWs) has been demonstrated for introducing biomolecules into a large number of cells in parallel. However, the microscopic understanding of how and when the nanowires penetrate cell membranes is still lacking, and the degree to which actual membrane penetration occurs is controversial. Here we present results from a mechanical continuum model of elastic cell membrane penetration through two mechanisms, namely through "impaling" as cells land onto a bed of nanowires, and through "adhesion-mediated" penetration, which occurs as cells spread on the substrate and generate adhesion force. Our results reveal that penetration is much more effective through the adhesion mechanism, with NW geometry and cell stiffness being critically important. Stiffer cells have higher penetration efficiency, but are more sensitive to NW geometry. These results provide a guide to designing nanowires for applications in cell membrane penetration.

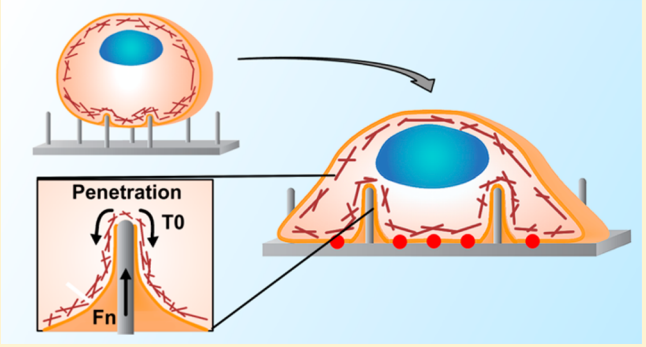

KEYWORDS: *Nanowire, cell membrane, penetration mechanism, mechanical model*

Direct access into a cell's intracellular space is essential for many therapeutic and scientific applications,[1−5] but the 4−6 nm thick plasma membrane presents a challenging barrier that prevents most external species from accessing the cytosol.[6,7] Of particular interest are one-dimensional systems which can provide direct access to the cell's interior by penetrating the cell membrane.[7−10] Nanowires (NW) have recently been demonstrated to be highly effective for intracellular detection of biochemical activity,[11] measurement of cellular electrical properties,[12] and intracellular delivery of various biological effectors (e.g., nucleic acids, proteins, and small molecules).[1,13−16] This nanoscale physical membrane penetration circumvents conventional biochemical pathways to deliver materials into the cell, and may avoid accompanying degradation routes such as endocytosis.[17−19] Large, delicate, or functional materials can now be directly delivered into the cytosol. Despite these successes, the basic question of how and when a nanowire actually penetrates a cell is not well understood, and there is still considerable controversy over whether the nanowires actually penetrate the cell membrane, or if cells simply engulf the NWs.[20−22] Indeed recent TEM studies suggest that penetration is rare, if it occurs at all.[22] This lack of understanding complicates the design of nanowire arrays and new cell-penetrating structures.[6,23−26]

To elucidate the possible penetration mechanisms, here we use a continuum elastic cell mechanics model to address how penetration occurs, and explore the characteristics that affect penetration. We consider cells cultured onto a vertical nanowire array with no external force applied. Under this scenario, there are two likely mechanisms for membrane failure: the first one is an "impaling mechanism", in which penetration is driven by cellular gravitational force during the initial cell plating, and the second one is the "adhesion mechanism", in which cells adhere to the substrate and the adhesion force induces penetration.[27] We used a mechanical model allowing for large-scale cell deformations to calculate tension within the lipid membrane under different loading scenarios. Our results reveal that, for typical NWs with radius of 50 nm, membrane penetration requires forces in the order of nN, which are roughly an order of magnitude higher than those expected from gravitational forces, implying that impaling penetration is difficult without using externally supplied force or sharp NWs with radius <10 nm. On the other hand, if a cell is adherent to the substrate, tension and strain are better localized at the NW−membrane contact interface, yet we find similar required penetration forces. However, cell−substrate adhesion can generate stronger forces, making penetration more likely, yet this is highly dependent on NW array geometry and cell rigidity. Stiff cells

Received: August 26, 2013
Revised: November 8, 2013
Published: November 15, 2013

 © 2013 American Chemical Society dx.doi.org/10.1021/nl403201a | *Nano Lett.* 2013, 13, 6002−6008

are easier to penetrate, but are also more sensitive to changes in NW array geometry (NW height or spacing). These models provide a framework to understand cell−NW interfaces and membrane penetration processes and provide nanomaterial design guidelines for direct access into a variety of different cell types.

The two proposed scenarios are based on the experimental observation of cell−NWs interface profiles (For all the abbreviation terms, see Supporting Information [SI], S1, Table S1). The SEM image in Figure 1a shows a spherical cell (Chinese hamster ovary cell, CHO cell) initially landing onto the NWs, and Figure 1b shows the cell spreading onto the substrate after 12 h, where the cell membrane closely wraps around NWs. In the impaling mechanism, the cell's initial state is assumed to be spherical as the cell first contacts the array

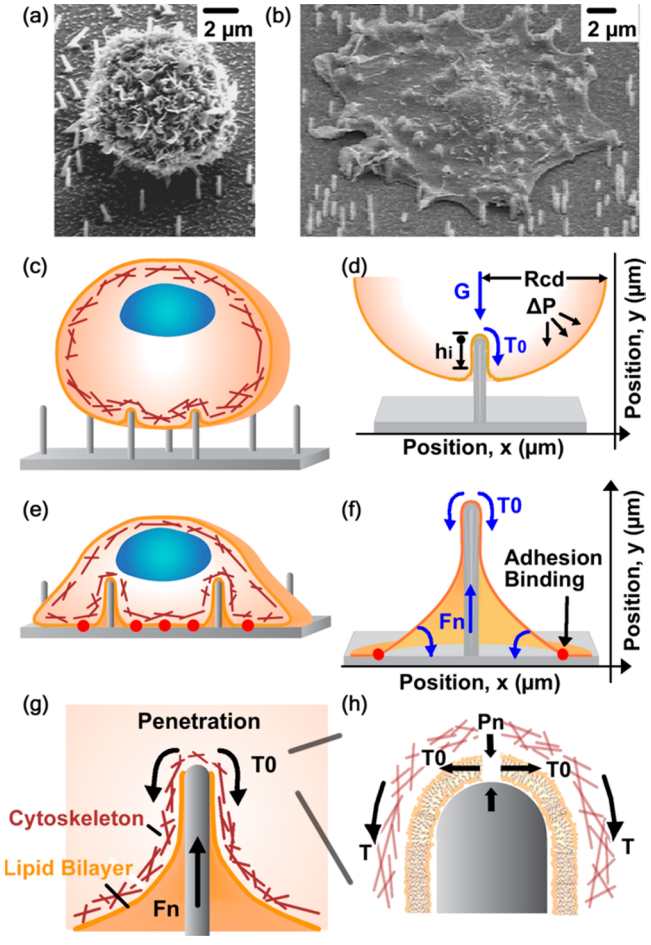

Figure 1. Schematic of penetration mechanisms and mechanical models. SEM images showing (a) a spherical cell (Chinese hamster ovary cell, CHO cell) initially landing onto NWs, and (b) CHO cell spreading and adhesion to the substrate, where the cell membrane closely wraps around NWs. (c, d) Impaling mechanism: nanowire penetration occurs as a cell lands on a bed of nanowires. In the presence of cellular gravity, the cell membrane undergoes large-scale deformations due to nanowire indentation, while the cell body maintains a constant volume. (e, f) Adhesion mechanism: nanowire penetration occurs as cells adhere to the substrate, inducing a localized vertical force between the membrane and the nanowire. (g) Schematic of cell membrane including both cytoskeletal elements and the fluid lipid bilayer membrane. (h) Cytoskeletal components of the cell oppose the vertical force from the nanowire, compressing the lipid bilayer which fails when the lateral tension reaches a critical value.

(Figure 1c, d). From this position, the cell membrane deforms as the cell wraps around the nanowires by the net gravitational and buoyancy force. We assume that for the time scale over which this process occurs there is negligible volume change within the cell, therefore NW indentation creates a uniformly distributed tension throughout the cell membrane due to the hydrostatic pressure inside the cell.[28,29] With sufficient externally applied force or sharp nanowires, this may lead to membrane rupture.

Alternatively, the cell may rupture through an "adhesion mediated" process. In this case the cell does not rupture immediately upon plating, but continues to deform around the nanowires until it eventually makes contact with the substrate surface (Figure 1e, f).[27] The surface interaction is assumed to be attractive, which may arise from both van der Waals interactions[30] or active processes such as receptor binding[31] and focal adhesions.[32,33] This interaction energy encourages additional membrane attachment, drawing the membrane taut against the NW and inducing a membrane tension. Membrane rupture may then occur, depending upon the membrane−substrate contact geometry, membrane stiffness, stress concentration at the NW tips, and NW geometry.

The mechanics of the cell membrane are a combination of the lipid membrane and underlying cytoskeleton. Although NWs cannot easily exert lateral tension on the lipid bilayer since the bilayer is a two-dimensional fluid in-plane,[34] the cytoskeletal elements can provide a stiffer mechanical layer against which the lipid bilayer can be compressed (Figure 1g, h).[35,36] This combined membrane is modeled as a single isotropic elastic sheet, where the elastic modulus encompasses both the cytoskeleton and lipid bilayer,[29,37] which has been widely applied to modeling the mechanics of red blood cells.[29,38,39] The observed Young's modulus (E) of cell membranes varies widely between 10 and 200 MPa,[40,41] which we try to capture by examining cells with soft, regular, and stiff membranes of 16 MPa (roughly corresponding to pure lipid bilayers), 48, and 144 MPa (roughly corresponding to red blood cells), denoted by $E/3$, E, and $E*3$ (SI, S2).

Membrane penetration will occur when a nanowire generates sufficient tension within the lipid bilayer to cause rupture (SI, S2), which may or may not pierce the cortical cytoskeleton. Lipid membrane failure has been studied extensively by pipet aspiration,[42] AFM,[43−45] and molecular dynamics simulations.[7,46] This behavior is often modeled by activation energy theory.[42,43]On the basis of this theory, thermally activated molecular-scale defects arise and vanish spontaneously in membranes, with the steady-state hole formation rate affecting the rupture probability. Membrane tension lowers the activation energy for hole formation, and thus increases the failure rate. Here we assume membrane penetration occurs within a period of one hour on the basis of experimental evidence,[1,13] which corresponds to a critical tension (T^*) for cell membrane rupture of 5.6 ± 2.7 mN/m (SI, S2). The failure tension is actually fairly insensitive to the time window chosen. For instance, varying the waiting time from 5 min to 24 h only results in a change of critical tension from 6.4 ± 2.9 mN/m to 5.0 ± 2.3 mN/m; thus, the particular time scale for failures does not greatly affect the outcome of subsequent calculations. For most figures in this paper a yellow-colored band is used to indicate this penetration tension regime (T^* >5.6 mN/m), with larger tensions implying higher penetration likelihood. Our calculated value agrees well with those of Evans et al., where lipid membrane rupture tensions were measured to be 1−10

dx.doi.org/10.1021/nl403201a | Nano Lett. 2013, 13, 6002−6008

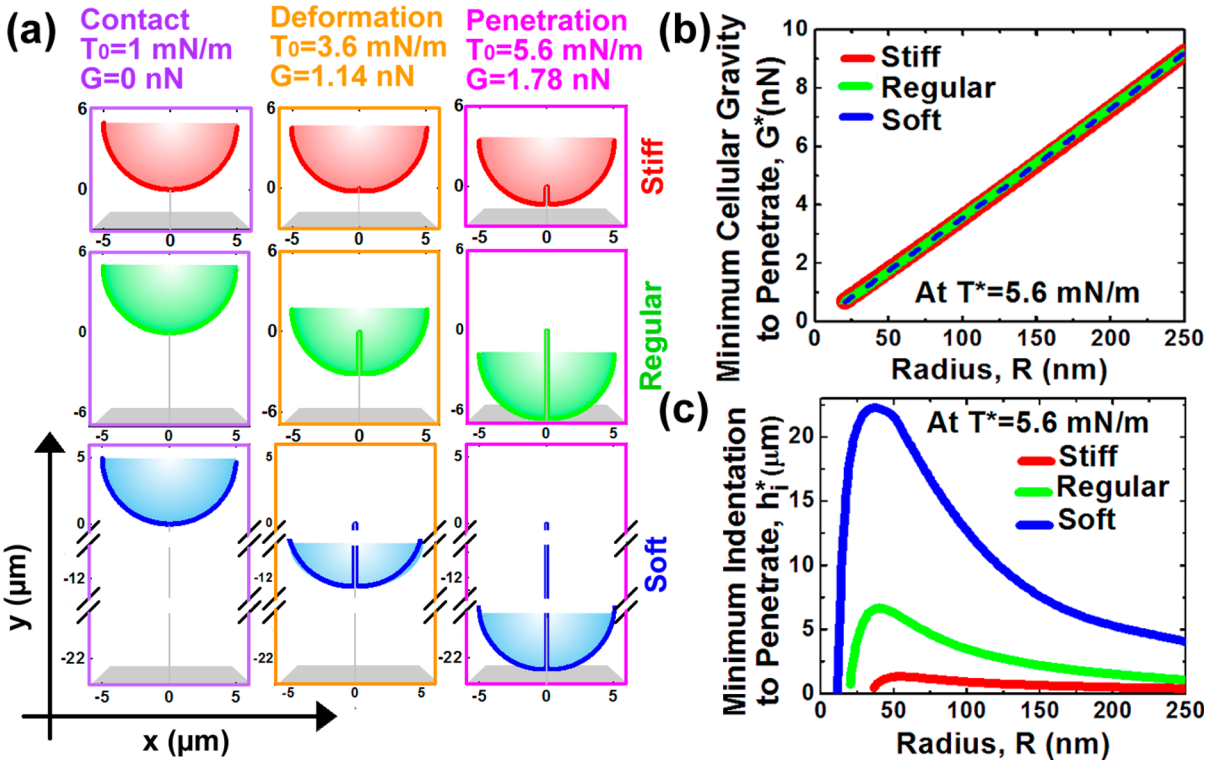

Figure 2. Membrane penetration through the impaling mechanism. (a) Evolution of the membrane profiles and tensions as the cells deform on the NW (R = 50 nm) for three different cellular gravities (0, 1.14, and 1.78 nN) and cell stiffnesses. Penetration requires driving forces on the scale of nN as well as large-scale indentation. (b) The minimum cellular gravity, G, and (c) indentation distance, h_i*, (c) to achieve penetration (T* = 5.6 mN/m) at varying NW radius. Lower indentations are needed at small NW radius (<50 nm) due to membrane bending energy.

mN/m at low loading rates.[42] The correlation of the critical penetration tension and time scale is shown in SI, Figure S2.

Here we calculate the criteria for the impaling mechanism where gravity induces penetration as a spherical cell settles onto the nanowire. Under a net cell gravitational force G typically on the order of 10−100 pN,[29,47,48] the cell is axisymmetrically indented by a nanowire represented by a cylindrical probe with a hemispherical tip (Figure 1c, d). The net force balance is given by:[29]

$$G = \Delta P(\pi R_{cd}^2) - 2\pi R_{cd} T_0 \quad (1)$$

where G is the net cellular gravity, ΔP is internal hydrostatic pressure inside the cell, R_{cd} is the equatorial radius of the cell that varies with membrane deformation, and T_0 is the tension on the cell membrane at the NW tip position. The net membrane tension T_0 comprises three parts: the indentation tension (T_a) arising from cell membrane area expansion during deformation, the bending tension ($T_{bending}$) due to membrane curving around the tip, and an intrinsic membrane tension at zero deformation (~1 mN/m).[28] The membrane shape and tension T_0 are then calculated by balancing membrane tension and hydrostatic pressure given by the Young−Laplace equation under the constraint of constant volume, which are solved numerically (SI, S3). This model is valid for nonadherent cells[29] where the hydrostatic pressure is uniformly distributed.

We start by analyzing the case of a typical single nanowire (R = 50 nm) indenting into a cell. Figure 2a shows the membrane deformation profile for the three different cell stiffnesses for T_0 = 1 (zero deformation), 3.6, and 5.6 mN/m (penetration), corresponding to gravitational forces of 0, 1.14, and 1.78 nN, respectively. As indicated in Figure 2a, the stiff cell requires 1.78 nN force and an indentation distance $h_i \approx 1$ μm to reach T_0 = 5.6 mN/m for penetration. Regular and soft cells require similar force (~1.78 nN), but much larger indentation distances (regular: $h_i \approx 5$ μm, and soft: $h_i > 20$ μm), suggesting that very tall, high-aspect ratio NWs are required for penetration in these cases. Note that these forces are roughly an order of magnitude higher than those expected to be generated from gravitational forces, implying that this mechanism is unlikely for typical NW with R = 50 nm unless external force is applied.

Penetration can be improved by using sharper NWs. The minimum force (G*) and indentation distance (h_i*) required to induce membrane penetration at varying NW radius are shown in Figure 2b,c. From the figure, G* decreases linearly with decreasing NW radii, and cells of different stiffness show negligible differences between them. On the other hand, the required indentation distance varies significantly. As tip radius decreases from 250 to 10 nm, the required h_i* increases, reaching a maximum at around 50 nm, at which point the trend reverses and h_i* decreases rapidly. This transition occurs due to the increasing importance of bending energy due to the bilayer curving around the NW tip. For larger NWs, the dominant component of T_0 is caused by membrane area expansion during deformation. For smaller NWs very little overall area change occurs even for large indentation depths, particularly for soft cells. However, for R < 50 nm the bending tension ($T_{bending}$) of the lipid bilayer becomes significant (SI, Figure S4a), and penetration requires a much shorter indentation distance. By using a sharp NW with R < 10 nm, the penetration force is on the order of 100 pN (Figure 2b), which is in the range of cellular gravity, and the required indentation distance is reasonably small (<1 μm, Figure 2c).

dx.doi.org/10.1021/nl403201a | Nano Lett. 2013, 13, 6002−6008

These results indicate the possibility of direct cell penetration through impaling by using very sharp nanowires (SI, Figure S4b,c). One example of this case is the spontaneous piercing of carbon nanotubes through lipid membranes, which could be induced by thermal motion.[7,49,50] These calculations are also consistent with atomic force microscope (AFM) experiments on nanoneedle penetrating mammalian cells that found penetration is easier for stiffer cell membranes with a significant actin cytoskeleton compared to soft membranes without appreciable actin.[35] For multiple NWs in an array, the gravitational force is distributed among multiple NWs, lowering the pressure at each NW. Therefore at higher density a "bed of nails" effect is achieved where the force is distributed so that penetration becomes impossible, thus making lower-density NW arrays preferable.

If a cell is not penetrated after distorting around the nanowire and settling onto the supporting substrate, it may adhere to the substrate (Figure 1e,f).[27] In this case the membrane–substrate surface interaction binds the membrane to the substrate and encourages additional membrane attachment,[32,51] clamping the membrane edges and inducing membrane strain and tension. This tension pulls the membrane taut against the nanowire tip and generates a normal force that may lead to membrane rupture (Figure 3a).[40]

Failure is determined from the initial cell membrane profile when it first contacts the substrate and the membrane tension as a substrate adhesion force is applied (SI S5). Unlike in conventional indentation of an elastic membrane where the initial membrane is flat before force is applied (SI S6),[52] in this case the membrane configuration as it deforms around the NW is unknown. To deal with this, we calculate a family of membrane profiles that have a total vertical force of 10 pN opposing the nanowire, approximating cellular gravity or protrusion forces (SI S7).[47,53,54] This method was taken since vertical force balance must be fulfilled at the moment that the cell contacts the substrate, regardless of the prior geometry, although the actual shape may not be as symmetrical as assumed here. The profiles are numerically calculated based upon an axisymmetric solution of the meridian and circumferential displacements by strain energy minimization under the constraint of zero displacement at the point of contact.[52,55] The membrane's strain energy relation is described by Mooney strain energy function by assuming the cell membrane is an isotropic, incompressible elastic material (SI S6).[38,39] Each cell stiffness results in a particular membrane profile, with representative shapes for different cell stiffnesses ($E*3$, $E*2$, E, $E/2$, and $E/3$) shown in Figure 3b. As expected, stiff cells ($E*2$ and $E*3$) adopt a flatter shape, while soft cells ($E/2$ and $E/3$) are distorted significantly, closely engulfing the NW for even this modest force. Similar membrane engulfment around NWs is observed experimentally (SI S8), supporting this choice of approach.[15,20−22]

At this point the cells begin to generate substrate adhesion forces, creating additional tension within the membrane. The contact point is taken to be fixed (e.g., the focal adhesion does not slide), and adhesion force is uniformly distributed around the contact circumference. The initial membrane shapes are taken as zero tension states, accounting for membrane relaxation. The adhesion force is then applied at the contact points, and then resulting membrane tension is calculated using the same mathematical formalism (SI, S9).

The total vertical force (F_n) between the membrane and nanowire is the integral of the adhesion-induced tension along

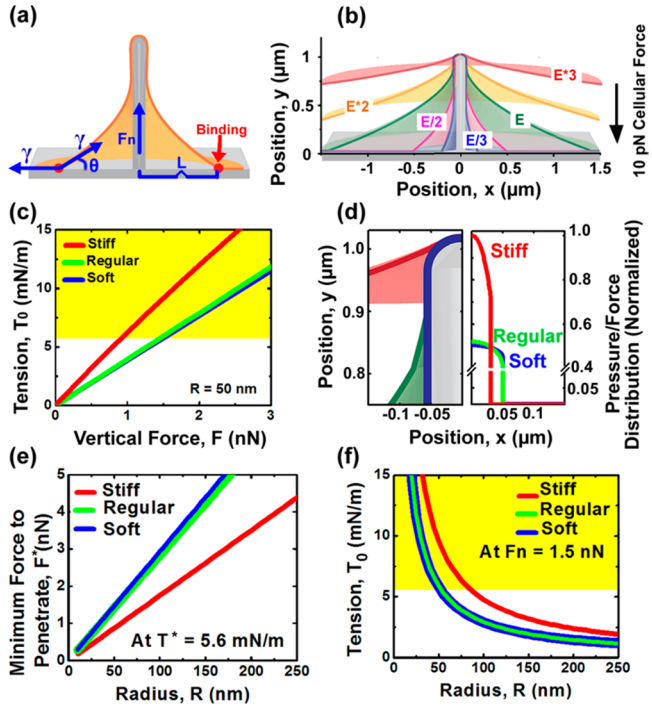

Figure 3. Membrane penetration through the adhesion mechanism. (a) Schematic of the mechanical model of cell–substrate adhesion forces and membrane geometry. (b) Initial membrane shapes upon contact for several different cell stiffnesses. The cell membrane is assumed to initially deform on NWs under a cellular gravity of 10 pN. (e) The tension (T_0) on the membrane at the nanowire tip (R = 50 nm) rises with increasing vertical force (F) in a near-linear manner for all three cell stiffnesses. (f) The higher tension observed in (c) for stiff cells arises due to stress concentration. The membrane profiles (left) show complete NW engulfment for the regular and soft cells, and only partial contact for the stiff cell. This results in a higher pressure at the tip (right). (g) The minimum vertical force for penetration increases linearly with increasing NW radius. (h) Conversely at a fixed 1.5 nN vertical force, membrane tension decreases rapidly as NW radius increases. Penetration becomes difficult for R > 150 nm. In (b, e, and f), NW radius is 50 nm. The penetration criterion (tension > 5.6 mN/m) is indicated as a yellow band.

the circumference of membrane–substrate contact circumference (Figure 3a): $F_n = 2\pi L\gamma \sin\theta$, where θ is the contact angle between membrane and substrate, and L is the contact distance between the initial cell–substrate contact point and the nanowire. The adhesion energy per unit area was taken from experimental measurements to be $W \approx 3 \times 10^{-5}$ J/m^2,[32,56,57] corresponding to a membrane adhesion tension $\gamma \approx 5 \times 10^{-4}$ N/m (SI, S10).[40,58] These parameters give some basic insight into enhancing penetration: increasing the NW height increases θ and the vertical component of the adhesion force, making penetration more likely. Similarly, increasing contact length (L) gives a larger circumference of membrane–substrate contact, resulting in larger net vertical force. For a NW array, L is limited to one-half of the average center-to-center distance of the nanowires, D, suggesting that lower nanowire density may be advantageous. Stiffer cells will have larger initial L, yet for tall NW or small D the membrane would never contact the substrate, resulting in a 'bed of nails' effect where penetration cannot occur through the adhesion mechanism.

Using this model we examined the amount of vertical force required to achieve the critical failure tension within the membrane, F^* (Figure 3c, d). In this situation the lipid bilayer

dx.doi.org/10.1021/nl403201a | Nano Lett. 2013, 13, 6002−6008

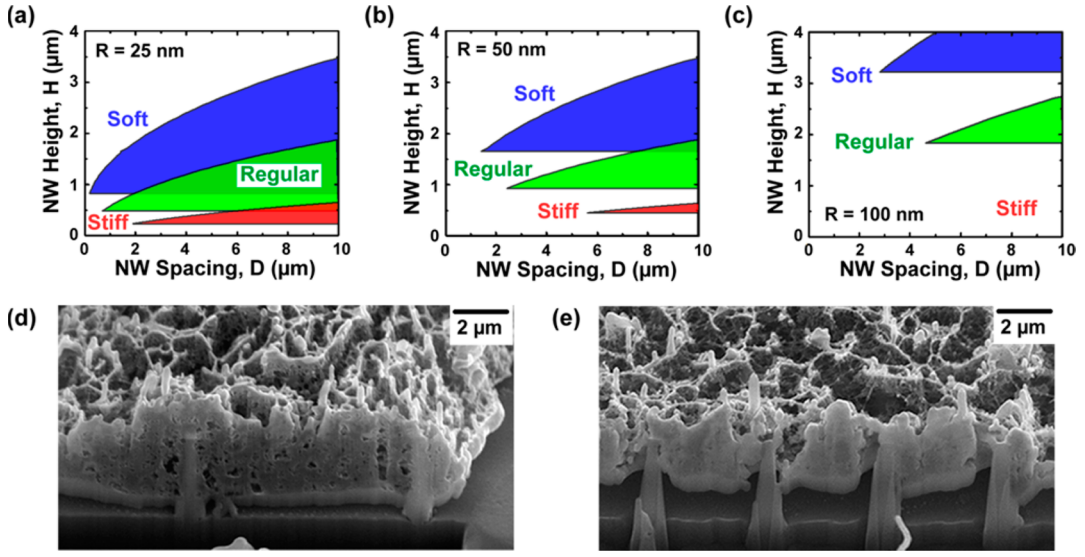

Figure 4. Effect of membrane stiffness and NW geometry on penetration. (a–c) The feasible penetration regimes for NW height and NW spacing. Stiff cell requires a much lower threshold of NW height to achieve penetration but has a narrower penetration regime (red). Long NW or reduced NW spacing can easily prevent the stiff cell from contact with the substrate and hence limit the penetration through adhesion mechanism. The soft cell has a wider penetration regime (blue), but it requires longer NWs for penetration. NW radius is 25 nm in (a), 50 nm in (b), and 100 nm in (c). (d–e) Focused-Ion-Beam milling reveals CHO cell membrane–NWs interface. (d) Cells greatly deform and wrap around the NWs, making contact with substrate, (e) while the decreased NW spacing lifts the cell away from substrate. Spacing is 5 μm in (d), and 2 μm in (e).

is compressed between the NW tip and the cytoskeleton, resulting in a lateral tension. The membrane tension T_0 at the nanowire tip increases nearly linearly with vertical force (F_n), with failure occurring at $F_n \approx 0.8–1.5$ nN for a 50 nm NW, which is very close to the conditions for the impaling mechanism. However, on the basis of previous measurements of cell–substrate adhesion energy[32,56,57] the cell is estimated to generate adhesion forces in the range of 0.1–5 nN (SI, S10). The predicted adhesion force is much stronger than the gravitational force discussed earlier, and therefore more likely to result in penetration, even though the required penetration forces are similar between the two mechanisms.

Results in Figure 3d reveal that stress concentration at the NW affects stiff cells much more than soft cells. The membrane profiles at the NW tips are shown in the left panel, with the corresponding pressure distribution in right panel (SI, S9). Stiff cells (red) adapt flatter membrane profiles with NW, and thus have smaller membrane contact area with the NW tip. This creates higher stress concentration at the NW tip compared to the softer membranes, and hence penetration requires less penetration force (~0.88 nN). On the other hand, the regular cell (green) and soft cell (blue) both have their membrane covering the entire NW tips, in which case the stress is distributed on a larger area and requires larger penetration force (~1.42 nN). Note that in all cases, the amount of membrane deformation required is much less than in the impaling model (SI, S11).

The NW radius also plays an important role in penetration force. As shown in Figure 3e, the minimum vertical force required (F^*) to reach a critical penetration tension (T^*) of 5.6 mN/m increases linearly with NW radius, rather than with surface area. The penetration force is generally on the order of nN for radii larger than 50 nm. Conversely, the tension generated at a fixed 1.5 nN vertical force decreases rapidly as NW radius is increased (Figure 3f). For NW radii of 150 nm and above, penetration becomes unlikely under the assumed conditions.

Next, we consider which geometric NW designs will promote cell penetration for different cell stiffnesses. The penetration regimes for NW radius (R), height (H), and spacing (D) are indicated in Figure 4a–c, which serve as approximate design guides of NW geometry for different cell types. For R = 50 nm (Figure 4b), stiff cells (red) require a much lower threshold of NW height (~0.46 μm) to achieve penetration than softer cells. However, they also require a lower NW density and have a narrow regime of height and spacing which lead to penetration. On the lower boundary, penetration is not observed for NWs shorter than 0.46 μm or for spacing less than 5.6 μm, because in these cases the adhesion force is not sufficient to induce penetration. On the other hand, on the upper boundary NWs longer than 0.7 μm do not cause penetration due to the 'bed of nails' effect that prevents the membrane from contacting the substrate. This is supported by SEM results on CHO cells showing that reduced NW spacing prevents cell–substrate contact (Figure 4d,e).

Soft cells have a wider penetration regime (blue), but require NWs longer than 1.6 μm to induce penetration. The width of the penetration regime changes more slowly as the NW spacing is reduced from 10 to 2 μm (Figure 4b) compared to stiff cells, and even for close NW spacing D = 2 μm, penetration can still be observed. Penetration into soft cells is thus less sensitive to spacing, even though it is more difficult to penetrate in general. For NW radius = 25 nm (Figure 4a), all three types of cells have larger penetration regimes, with lower penetration thresholds of both NW height and spacing, showing that penetration is a strong function of NW radius. As NW radius increases to 100 nm (Figure 4c), penetration becomes more difficult. In this case, the stiff cell's penetration regime disappears, and the regimes of regular and soft cells become much narrower. In actual experiments with a distribution of NW radii it may only be NWs with the smallest radii that actually penetrate.

Our results suggest that, for typical NWs with radii on the order of 50 nm, membrane penetration requires driving forces

dx.doi.org/10.1021/nl403201a | *Nano Lett.* 2013, 13, 6002–6008

at the nN scale, which is generally an order higher than the net cell gravitational force. We therefore conclude that nanowire penetration is unlikely to occur in the absence of external force, unless the NW radius is as small as ~10 nm. On the other hand, cells may generate adhesion forces on this scale, thus adhesion-mediated penetration is feasible within certain predicted regimes of cell stiffness and nanowire geometry.

Our model has assumed that the cell membrane properties remain constant, while in reality the membrane can undergo viscous relaxation and is continuously rearranging by active processes. A more advanced model would be required to treat the penetration accounting for the kinetics of a viscoelastic membrane and cellular adhesion. Nonetheless, we believe that by choosing conservative values in our model and using reasonable assumptions, we have described the general regimes in which membrane penetration could be possible, and perhaps where it is unlikely to occur. We believe that understanding these regimes and the cellular and NWs characteristics that define them will ultimately lead to a better understanding of nanobio interactions and the rationally guided design of future tools for nanobioscience.

■ ASSOCIATED CONTENT

Ⓢ Supporting Information

Additional experimental details, experimental methods, calculation methods, supplemental figures, supplemental discussion, and table of abbreviations. This material is available free of charge via the Internet at http://pubs.acs.org.

■ AUTHOR INFORMATION

Corresponding Author

*E-mail: nmelosh@stanford.edu. Telephone: (650) 724-3679. Fax: (650) 736-1984. Address: 476 Lomita Mall, McCullough Bldg. Stanford, CA 94305.

Notes

The authors declare no competing financial interest.

■ ACKNOWLEDGMENTS

We thank the Yi Cui and Sarah Heilshorn Laboratories for use of equipment and experimental advice. This work was supported by the National Institutes of Health Grants R21 MH091471 (C.C.G), the United States Israel Binational Science Foundation Grant 2007425 (C.C.G), the Coulter Foundation (N.M. and C.C.G) and a Stanford BioX-Neuroventures Award (N.M. and C.C.G). X.X. acknowledges the China Scholarship Council (File NO. 2009638027) for support. A.X. acknowledges the NSF Graduate Fellowship for support.

■ ABBREVIATIONS

CHO cells, Chinese hamster ovary cell; SEM, scanning electron microscope; FIB, focused Ion beam; nanowires, NWs. For all the abbreviation terms in equations, see SI S1, Table S1

■ REFERENCES

(1) Shalek, A. K.; Robinson, J. T.; Karp, E. S.; Lee, J. S.; Ahn, D. R.; Yoon, M. H.; Sutton, A.; Jorgolli, M.; Gertner, R. S.; Gujral, T. S.; MacBeath, G.; Yang, E. G.; Park, H. *Proc. Natl. Acad. Sci. U.S.A.* **2010**, *107*, 1870−1875.
(2) Stephens, D. J. *Proc. Natl. Acad. Sci. U.S.A.* **2001**, *98*, 4295−4298.
(3) Herweijer, H.; Wolff, J. A. *Gene Ther.* **2003**, *10*, 453−458.
(4) Angle, M. R.; Schaefer, A. T. *PLoS ONE* **2012**, *7*, e43194.
(5) Xie, C.; Lin, Z.; Hanson, L.; Cui, Y.; Cui, B. *Nanotechnology* **2012**, *7*, 185−190.
(6) Wong, I. Y.; Almquist, B. D.; Melosh, N. A. *Mater. Today* **2010**, *13*, 14−22.
(7) Pogodin, S.; Baulin, V. A. *ACS Nano* **2010**, *4*, 5293−5300.
(8) Chen, X.; Kis, A.; Zettl, A.; Bertozzi, C. R. *Proc. Natl. Acad. Sci. U.S.A.* **2007**, *104*, 8218−8222.
(9) Kim, W.; Ng, J. K.; Kunitake, M. E.; Conklin, B. R.; Yang, P. *J. Am. Chem. Soc.* **2007**, *129*, 7228−7229.
(10) Berthing, T.; Sørensen, C. B.; Nygård, J.; Martinez, K. L. *J. Nanoneurosci.* **2009**, *1*, 3−9.
(11) Na, Y.-R.; Kim, S. Y.; Gaublomme, J. T.; Shalek, A. K.; Jorgolli, M.; Park, H.; Yang, E. G. *Nano Lett.* **2013**, *13*, 153−158.
(12) Robinson, J. T.; Jorgolli, M.; Shalek, A. K.; Yoon, M.-H.; Gertner, R. S.; Park, H. *Nat. Nanotechnol.* **2012**, *7*, 180−184.
(13) Shalek, A. K.; Gaublomme, J. T.; Wang, L.; Yosef, N.; Chevrier, N.; Andersen, M. S.; Robinson, J. T.; Pochet, N.; Neuberg, D.; Gertner, R. S.; Amit, I.; Brown, J. R.; Hacohen, N.; Regev, A.; Wu, C. J.; Park, H. *Nano Lett.* **2012**, *12*, 6498−6504.
(14) Yosef, N.; Shalek, A. K.; Gaublomme, J. T.; Jin, H.; Lee, Y.; Awasthi, A.; Wu, C.; Karwacz, K.; Xiao, S.; Jorgolli, M.; Gennert, D.; Satija, R.; Shakya, A.; Lu, D. Y.; Trombetta, J. J.; Pillai, M. R.; Ratcliffe, P. J.; Coleman, M. L.; Bix, M.; Tantin, D.; Park, H.; Kuchroo, V. K.; Regev, A. *Nature* **2013**, *496*, 461−468.
(15) VanDersarl, J. J.; Xu, A. M.; Melosh, N. A. *Nano Lett.* **2012**, *12*, 3881−3886.
(16) Park, S.; Kim, Y.-S.; Kim, W. B.; Jon, S. *Nano Lett.* **2009**, *9*, 1325−1329.
(17) Kam, N. W. S.; Liu, Z.; Dai, H. *Angew. Chem., Int. Ed.* **2006**, *45*, 577−581.
(18) Gao, H.; Shi, W.; Freund, L. B. *Proc. Natl. Acad. Sci. U.S.A.* **2005**, *102*, 9469−9474.
(19) Shi, X.; Bussche, A. v. d.; Hurt, R. H.; Kane, A. B.; Gao, H. *Nat. Nanotechnol.* **2011**, *6*, 714−719.
(20) Berthing, T.; Bonde, S.; Sørensen, C. B.; Utko, P.; Nygård, J.; Martinez, K. L. *Small* **2011**, *7*, 640−647.
(21) Mumm, F.; Beckwith, K. M.; Bonde, S.; Martinez, K. L.; Sikorski, P. *Small* **2013**, *9*, 263−272.
(22) Hanson, L.; Lin, Z. C.; Xie, C.; Cui, Y.; Cui, B. *Nano Lett.* **2012**, *12*, 5815−5820.
(23) Tian, B.; Cohen-Karni, T.; Qing, Q.; Duan, X.; Xie, P.; Lieber, C. M. *Science* **2010**, *329*, 830−834.
(24) Duan, X.; Gao, R.; Xie, P.; Cohen-Karni, T.; Qing, Q.; Choe, H. S.; Tian, B.; Jiang, X.; Lieber, C. M. *Nat. Nanotechnol.* **2012**, *7*, 174−179.
(25) Xie, X.; Xu, A. M.; Leal-Ortiz, S.; Cao, Y.; Garner, C. C.; Melosh, N. A. *ACS Nano* **2013**, *7*, 4351−4358.
(26) Peer, E.; Artzy-Schnirman, A.; Gepstein, L.; Sivan, U. *ACS Nano* **2012**, *6*, 4940−4946.
(27) Qi, S.; Yi, C.; Ji, S.; Fong, C.-C.; Yang, M. *ACS Appl. Mater. Interfaces* **2009**, *1*, 30−34.
(28) Sen, S.; Subramanian, S.; Discher, D. E. *Biophys. J.* **2005**, *89*, 3203−3213.
(29) Verma, P.; Wong, I. Y.; Melosh, N. A. *Biointerphases* **2010**, *5*, 37.
(30) Nir, S.; Andersen, M. *J. Membr. Biol.* **1977**, *31*, 1−18.
(31) Lee, F.-H.; Haskell, C.; Charo, I. F.; Boettiger, D. *Biochemistry* **2004**, *43*, 7179−7186.
(32) Cuvelier, D.; Théry, M.; Chu, Y.-S.; Dufour, S.; Thiéry, J.-P.; Bornens, M.; Nassoy, P.; Mahadevan, L. *Curr. Biol.* **2007**, *17*, 694−699.
(33) Wehrle-Haller, B.; Imhof, B. A. *Int. J. Biochem. Cell Biol.* **2003**, *35*, 39−50.
(34) Baoukina, S.; Marrink, Siewert J.; Tieleman, D. P. *Biophys. J.* **2012**, *102*, 1866−1871.
(35) Kagiwada, H.; Nakamura, C.; Kihara, T.; Kamiishi, H.; Kawano, K.; Nakamura, N.; Miyake, J. *Cytoskeleton* **2010**, *67*, 496−503.
(36) Alenghat, F. J.; Ingber, D. E. *Sci. Signal.* **2002**, *2002*, pe6−pe6.
(37) Evans, E. A.; Waugh, R.; Melnik, L. *Biophys. J.* **1976**, *16*, 586−595.
(38) Evans, E. A. *Biophys. J.* **1973**, *13*, 926−940.
(39) Skalak, R.; Tozeren, A.; Zarda, R. P.; Chien, S. *Biophys. J.* **1973**, *13*, 245−264.

(40) Hategan, A.; Law, R.; Kahn, S.; Discher, D. E. *Biophys. J.* **2003**, *85*, 2746−2759.
(41) Lulevich, V.; Zimmer, C. C.; Hong, H..; Jin, L.; Liu, G. *Proc. Natl. Acad. Sci. U.S.A.* **2010**, *107*, 13872−13877.
(42) Evans, E.; Heinrich, V.; Ludwig, F.; Rawiczy, W. *Biophys. J.* **2003**, *85*, 2342−2350.
(43) Butt, H.-J.; Franz, V. *Phys. Rev. E* **2002**, *66*, 031601.
(44) Loi, S.; Sun, G.; Franz, V.; Butt, H.-J. *Phys. Rev. E* **2002**, *66*, 031602.
(45) Obataya, I.; Nakamura, C.; Han, S.; Nakamura, N.; Miyake, J. *Biosens. Bioelectron.* **2005**, *20*, 1652−1655.
(46) Tieleman, D. P.; Leontiadou, H.; Mark, A. E.; Marrink, S.-J. *J. Am. Chem. Soc.* **2003**, *125*, 6382−6383.
(47) Godin, M.; Delgado, F. F.; Son, S.; Grover, W. H.; Bryan, A. K.; Tzur, A.; Jorgensen, P.; Payer, K.; Grossman, A. D.; Kirschner, M. W.; Manalis, S. R. *Nat. Methods* **2010**, *7*, 387−390.
(48) Bryan, A. K.; Goranov, A.; Amon, A.; Manalis, S. R. *Proc. Natl. Acad. Sci. U.S.A.* **2009**, *107*, 999−1004.
(49) Lacerda, L.; Raffa, S.; Prato, M.; Bianco, A.; Kostarelos, K. *Nano Today* **2007**, *2*, 38−43.
(50) Vakarelski, I. U.; Brown, S. C.; Higashitani, K.; Moudgil, B. M. *Langmuir* **2007**, *23*, 10893−10896.
(51) Carey, S. P.; Charest, J. M.; Reinhart-King, C. A. *Stud. Mechanobiol. Tissue Eng. Biomater.* **2011**, *4*, 29−69.
(52) Yang, W. H.; Hsu, K. H. *J. Appl. Mech.* **1971**, *38*, 227−230.
(53) Mogilner, A.; Rubinstein, B. *Biophys. J.* **2005**, *89*, 782−795.
(54) Kress, H.; Stelzer, E. H. K.; Holzer, D.; Buss, F.; Griffiths, G.; Rohrbach, A. *Proc. Natl. Acad. Sci. U.S.A.* **2007**, *104*, 11633−11638.
(55) Yang, W. H.; Feng, W. W. *J. Appl. Mech.* **1970**, *37*, 1002−1011.
(56) Sackmann, E.; Bruinsma, R. *ChemPhysChem* **2002**, *3*, 262−269.
(57) Boal, D.*Mechanics of the Cell*; Cambridge University Press: Cambridge, New York, 2002.
(58) Pietuch, A.; Janshoff, A. *Open Biol.* **2013**, *3*, 130084−130084.